Peripapillary Retinoschisis in Glaucoma: Association With Progression and OCT Signs of Müller Cell Involvement

Brad Fortune,[1] Kelly N. Ma,[2] Stuart K. Gardiner,[1] Shaban Demirel,[1] and Steven L. Mansberger[1]

[1]Discoveries in Sight Research Laboratories, Devers Eye Institute and Legacy Research Institute, Legacy Health, Portland, Oregon, United States
[2]Northwest Permanente, Portland, Oregon, United States

Correspondence: Brad Fortune, Discoveries in Sight Research Laboratories, Devers Eye Institute and Legacy Research Institute, 1225 NE Second Avenue, Portland, OR 97232, USA; bfortune@deverseye.org.

Submitted: February 20, 2018
Accepted: April 29, 2018

Citation: Fortune B, Ma KN, Gardiner SK, Demirel S, Mansberger SL. Peripapillary retinoschisis in glaucoma: association with progression and OCT signs of Müller cell involvement. *Invest Ophthalmol Vis Sci*. 2018;59:2818–2827. https://doi.org/10.1167/iovs.18-24160

Purpose. To examine demographic and clinical factors associated with glaucomatous peripapillary retinoschisis (PPRS) and assess its association with glaucoma progression.

Methods. Using a case control study design and longitudinal data from a cohort of 166 subjects with a diagnosis of glaucoma or glaucoma suspect, we compared functional, structural, clinical, and demographic characteristics between PPRS cases and controls.

Results. The frequency of PPRS was 6.0% (12 eyes from 10/166 subjects) with two eyes having PPRS in different sectors for a total of 15 retinoschisis events. There were no significant differences ($P > 0.05$) in age, sex, visual acuity, central corneal thickness, intraocular pressure, or presence of vitreous adhesion between PPRS and controls. However, eyes with PPRS tended to have a higher cup-to-disc ratio ($P = 0.06$), thinner RNFL ($P = 0.02$), and worse visual field mean deviation (MD, $P = 0.06$) than controls. The rate of RNFL thinning was faster in PPRS (average: −2.8%/year; range: −7.4% to 0.0%/year) than controls (−1.3%/year; range: −4.4% to 0.6%/year; $P = 0.021$). The rate of visual field MD change was faster in PPRS (−0.49 dB/year; range: −2.0 to 0.9 dB/year) than controls (−0.06 dB/year; range: −0.8 to 0.3 dB/year; $P = 0.030$). OCT scans showed hyperreflective structures spanning the PPRS whose morphology and spacing (50 ± 7 µm) are consistent with Müller glia, causing signal attenuation casting "shadows" onto distal retina.

Conclusions. This is the first report showing that glaucomatous PPRS is associated with a faster overall rate of RNFL thinning and visual field deterioration and to specifically identify OCT signs of Müller cell involvement.

Keywords: glaucoma, peripapillary retinoschisis, optical coherence tomography, retinal nerve fiber layer, optic nerve head, Müller glia

Retinoschisis refers to an abnormal splitting of the sensory retina. In X-linked juvenile retinoschisis (XLRS), it occurs as a result of inherited mutations in the *RS1* gene, which encodes retinoschisin, a protein expressed and secreted by photoreceptors and thought to be involved in cell-cell adhesion, organization of retinal layers during development, and maintenance of the photoreceptor-to-bipolar cell synapse.[1–4] With an estimated prevalence of 0.4% to 2.0%, XLRS is less common than senile or degenerative (acquired) retinoschisis, which is observed in approximately 7% of persons aged older than 40 years and most commonly found bilaterally in the inferotemporal quadrant of the far peripheral retina.[5,6] Because XLRS probably impacts the entire retina, often with profound effects on macular structure and function in affected young males, its prognosis is considerably worse than that of senile retinoschisis, which rarely requires treatment.

Retinoschisis can also occur in the macula as a result of optic nerve head (ONH) structural abnormalities, such as in optic nerve pit, optic nerve coloboma, tilted disc syndrome, morning glory syndrome and high myopia.[7–10] A recent series of case reports has led to wider recognition that retinoschisis sometimes develops in the macula and peripapillary retina as a result of glaucomatous ONH structural changes (such as optic "cupping") without any detectable optic disc pit, tilted disc or high myopia.[11–16] Some of these initial case reports were based on incidental findings from optical coherence tomography (OCT) scans of the peripapillary retina, which showed that when retinoschisis did not extend to or involve the fovea, patients were asymptomatic and their retinoschisis often resolved spontaneously.[13,14,17–20] However, because this type of peripapillary retinoschisis (PPRS) commonly occurs within the retinal nerve fiber layer (RNFL), these and other authors have stressed the important point that caution is warranted when interpreting transient changes in OCT-derived measurements of RNFL thickness, particularly during any rapid decline associated with resolution of the retinoschisis, which could be potentially mistaken for rapidly progressing glaucomatous RNFL thinning.[13,14,18,20–23]

Subsequent to the initial case reports, larger studies have shown that PPRS is more common in patients diagnosed with glaucoma or as glaucoma suspects than in age-matched controls with healthy eyes.[20–22] These studies also suggest that PPRS in glaucoma occurs most commonly in sectors where RNFL defects already exist and/or that resolution of PPRS often reveals a glaucomatous RNFL defect.[20,21] However, it is not known whether PPRS represents a risk for glaucoma progression.

The pathogenesis of PPRS also remains unclear. While some reports have suggested vitreo-retinal traction may be involved,[22,24,25] others have found no such association[23] and this would not adequately explain the higher prevalence of PPRS in glaucoma. Others have speculated that PPRS might result from abnormalities of the interface between the vitreous and the anterior surface of the ONH[11,12,14,16] and/or that defects of the lamina cribrosa might be contributory factors.[21,26] Supporting the former hypothesis, a proteomic analysis found that the source of the fluid that filled the schisis cavity in a case of advanced glaucoma was most likely the vitreous humor.[27]

It has long been thought that Müller cells, the radial macro glia of the retina, were somehow important to the pathogenesis of XLRS,[28,29] but this notion has not been considered in the context of glaucomatous PPRS. Yet it is known that Müller cells exhibit signs of reactive gliosis in human glaucoma[30] and that targeted ablation of Müller cells during development results in decreased resistance to tensile forces and spontaneous schisis within the ganglion cell layer (GCL) of the inner retina.[31]

Here we evaluate longitudinal OCT scans of the ONH and peripapillary retina in a cohort of glaucoma patients and suspects to determine the proportion of eyes with detectable PPRS, the demographic and clinical factors associated with PPRS, its association with glaucoma progression, and the degree to which signs of Müller cell reactivity are present in PPRS.

Methods

The Portland Progression Project (P3) is an ongoing prospective longitudinal study of the course and risk factors for glaucomatous progression, conducted at the Devers Eye Institute, Portland, Oregon.[32,33] Inclusion criteria were a diagnosis of primary open-angle glaucoma, and/or likelihood of developing glaucomatous damage (e.g., ocular hypertension with other risk factors such as an optic disc appearance suspicious for glaucoma and/or a family history of glaucoma), as determined by each participant's physician. A visual field defect was not a requirement for study entry, nor was significant RNFL thinning. Exclusion criteria were an inability to perform reliable visual field testing, best-corrected visual acuity worse than 20/40, cataract or significant media opacities, or other conditions or medications that may affect the visual field. Participants provided written informed consent once all the risks and benefits of participation were explained to them. All protocols were approved and monitored by the Legacy Health Institutional Review Board and adhered to the Health Insurance Portability and Accountability Act of 1996 and the tenets of the Declaration of Helsinki.

As part of the routine follow-up testing in this study, a trained ophthalmic technician performed standard automated perimetry (SAP) and OCT in both eyes of all participants every six months. SAP was performed at each visit using a Humphrey Field Analyzer (HFA II; Carl Zeiss Meditec, Dublin, CA, USA), with a size III stimulus, Swedish Interactive Threshold Algorithm (SITA) standard algorithm, and 24–2 test pattern. Visual field status was summarized using the mean deviation (MD) global index. OCT was performed at each visit with a spectral domain OCT instrument (Spectralis, Heidelberg Engineering, GmbH, Heidelberg, Germany). OCT scans were recorded in high resolution and follow-up mode (registered to the position of the first scan in each longitudinal series) as an average of 9–16 individual sweeps. OCT scans centered on the ONH included a radial star pattern comprised of 24 B-scans, each spanning 15° and consisting of 768 A-lines, as well as a single circumpapillary B-scan that was 12° in diameter and consisted of 1536 A-lines. The instrument's automated image segmentation algorithm identifies the anterior and posterior boundaries of the RNFL (i.e., the boundary between the vitreous and internal limiting membrane, ILM, and the boundary between the RNFL and ganglion cell layer, respectively). Experienced technicians refined the automated segmentations manually to correct obvious errors when present.[34] Peripapillary RNFL thickness was measured from the circumpapillary B-scan as the axial distance between the ILM and the posterior RNFL segmentations. Simultaneous stereo color photographs of the optic discs were obtained once per year (3-Dx; Nidek Co., Ltd., Gamagori, Japan; or Kowa Nonmyd WX^{3D}; Kowa Company, Ltd., Tokyo, Japan).

At the time of initiating this study of PPRS, the P3 cohort consisted of 166 individuals. To determine the proportion of eyes with PPRS, all ONH and circumpapillary OCT scans of all active participants were carefully reviewed. We identified 12 eyes of 10 P3 study participants with clear evidence of PPRS present at some point in their longitudinal series, confirmed by consensus of three authors (KNM, SLM, BF). In those eyes with evidence of active PPRS, additional OCT scans were obtained in a dense horizontal raster pattern over the area of PPRS (see "Results").

To evaluate the demographic and clinical features associated with PPRS, we compared characteristics of the 10 patients with PPRS to those of 30 randomly selected P3 participants without PPRS using a 1:3 case-control study design. We included visual field results obtained at the same visit when PPRS was detectable by OCT, as well as for the prior visit (6 months earlier) and for the first visit when OCT signs of PPRS had resolved (i.e., if resolution was observed). We documented the optic disc cup-to-disc ratio as well as features of the optic disc such as nerve fiber thinning, notching, or optic pit based on clinical exam notes and review of simultaneous stereo color optic disc photos through a stereoscopic viewer. The presence or absence of posterior vitreous adhesion to the surface of optic disc and/or peripapillary retina was assessed by review of the OCT scans. We evaluated the association of PPRS with the location and severity of any visual field abnormality, cup-to-disc ratio, intraocular pressure (IOP), visual acuity, central corneal thickness (CCT), the presence of vitreous traction, diagnosis (glaucoma or suspect), and ethnicity. Clinical characteristics between groups were compared using parametric and nonparametric statistical tests accordingly after applying the D'Agostino & Pearson omnibus normality test.

To compare progression between the group of eyes with PPRS and the group of 30 controls without PPRS, we calculated the rate of change for global average RNFL thickness (μm/year) and for SAP visual field MD (dB/year). For RNFL thickness, only data from the scan dates immediately preceding the onset of PPRS and immediately following resolution of PPRS were included, since measurements obtained between these time points would be artificially increased by the presence of PPRS. For SAP, all test dates were included from the visit that preceded onset of PPRS until the visit following resolution (inclusive). Generalized estimating equation (GEE) models were used to account for the fact that some eyes in the PPRS group had more than one PPRS event. Analyses were performed using Prism (version 5; GraphPad Software, Inc., La Jolla, CA, USA) and the R language and environment for statistical computing (Version 2.15.3; R Core Team, Vienna, 2013, http://www.R-project.org/).

OCT images from one adult rhesus macaque monkey with idiopathic bilateral optic atrophy[35,36] were also included for analytical comparison. To acquire those images, all procedures adhered to the Association for Research in Vision and Ophthalmology's Statement for the Use of Animals in

Investigative Ophthalmology & Visual Science

Ophthalmic and Vision Research and were carried out in strict accordance with the recommendations in the Guide for the Care and Use of Laboratory Animals of the National Institutes of Health and were approved and monitored by the Institutional Animal Care and Use Committee (IACUC) at Legacy Health (USDA license 92-R-0002 and OLAW assurance A3234–01).

Results

Patient Demographics

A total of 10 patients (12 eyes) with PPRS were identified in the P3 cohort of 166 study participants. Thus, the proportion of P3 study participants with OCT evidence of PPRS was 6.0% (10/166 persons). The average duration of follow-up in this group was 60 months (range 4–96 months from onset of PPRS or from first OCT exam to most recent follow-up OCT exam). Although some eyes had evidence of PPRS visible in OCT scans at study entry and/or persisting at the most recent follow-up visit, there were eight PPRS events in seven eyes with clear onset and resolution, from which we determined an average PPRS duration of 23 months (range: 5.6 to 42.2 months). It should be noted that one additional PPRS, which had not yet resolved at the time of the most recent visit, has persisted for 5 years. In total, there were 15 distinct PPRS events in these 12 eyes because 2 eyes (of 2 patients) had multiple, separate PPRS events (details below).

The demographic and clinical characteristics of the two study groups are presented in the Table. There was no significant difference in age, gender, visual acuity, IOP, CCT or whether IOP was at goal between the PPRS group and the control group. However, the group of eyes with PPRS had a tendency toward being at a slightly more advanced stage of disease just prior to the onset of PPRS than did the control group at study entry, with marginally larger cup-to-disc ratio ($P = 0.06$), worse SAP visual field MD ($P = 0.09$) and thinner RNFL ($P = 0.02$, Table).

Peripapillary Retinoschisis Clinical Characteristics

We found that PPRS is generally difficult to appreciate by clinical examination or by color fundus photography, consistent with previous reports.[14,21] Figure 1 presents an example of an eye with PPRS. The area of PPRS is difficult to discern in the color fundus photograph (Fig. 1A), but appears as a slightly elevated area extending from the superior pole of the optic disc with exaggerated striae that follow the course of the RNFL bundles toward the disc. The area of PPRS and its boundaries are more readily visible in the scanning laser ophthalmoscope (SLO) infrared fundus reflectance image (Fig. 1B) as previously reported. One aspect of heightened visibility is the greater prominence of striae, reflections that follow the course of RNFL bundles toward the ONH, overlying a darkened area of the infrared reflectance image contiguous with the optic disc.[20,21,23] In this eye, the area of PPRS involved more than 120° (4 clock hours) of the superior pole as judged by its intersection with the circumpapillary OCT B-scan (Figs. 1B, 1C, red arrowheads). The outer retina was also involved in this eye (Fig. 1C, green arrow). Approximately 3 years later, this PPRS persisted, however its overall height had begun to decrease, particularly because the schisis within the RNFL had begun to resolve, although the schisis at the posterior boundary of the outer plexiform layer (OPL) had become wider (laterally, Fig. 1E). The extent of the schisis overall and involvement of each layer varied with distance from the ONH, as can be seen by comparison of Figures 1F to 1G.

PPRS was most commonly limited in extent to one to two clock hours radially around the ONH. However, in some eyes, PPRS extended dramatically to include an area as large as 5 clock hours (the case shown in Fig. 1; e.g., was over 120° wide). The range of PPRS extent measured in degrees at the intersection with the circumpapillary B-scan was 30° to 150°, with a median value of 45°. PPRS was observed most commonly in the superior quadrant: 10/15 (67%) of the separate PPRS events were observed in the superior quadrant, while 5/15 (33%) were observed in the inferior quadrant; none were observed within the temporal or nasal quadrant (without being primarily located along either the superior or inferior pole with extension into the temporal or nasal quadrant). All instances of PPRS included at least one major blood vessel within the area of the schisis.

PPRS was isolated to the inner retina (RNFL and GCL) in 9/12 eyes (75%) but additionally involved the outer retina (spanning the OPL boundary) in 3/12 eyes (25%). In the latter cases, there were particular visits during which only the outer retina exhibited schisis; however, with the benefit of longitudinal follow-up, it is clear that the same radial sectors show involvement of the RNFL at other time points. Figure 2 shows a series of longitudinal follow-up OCT scans in an eye that developed multiple PPRS events over time. At study entry, there was evidence of outer retinal involvement (spanning the OPL-ONL boundary) of the inferior quadrant, with little apparent involvement of the inner retina (Fig. 2B, white arrow). At the next visit 6 months later, the outer retinal schisis appeared to have narrowed but the inner retina at the same inferior location had clearly become involved (Fig. 2D, red arrow) and an entirely separate PPRS event had manifest within the RNFL of the temporal-superior sector (Fig. 2D, green arrow). Both locations gradually resolved over the next year (Figs. 2F, 2H), but 6 months later, the same temporal-superior sector RNFL schisis recurred (Fig. 2J, green arrow) and was contiguous with a severe outer retinal schisis, which spanned nearly the entire superior hemisphere (Fig. 2J, green arrowheads). This outer retinal schisis took longer to resolve than the RNFL schisis; when both appeared to be completely resolved 2.5 years later, there was clear evidence that progressive RNFL thinning had occurred, including protrusion of the major blood vessels anteriorly toward the vitreous (Fig. 2P, asterisks), a phenomenon previously reported.[37,38]

As inferred above, PPRS was observed in both eyes of 2/10 patients (20%), overlapping in time such that it presented bilaterally in both patients during at least one study visit. Figure 3 presents a series of longitudinal follow-up circumpapillary OCT scans for a patient with recurrent PPRS in one eye and bilateral presentation during at least one semiannual visit. At study entry, this patient's right eye shows PPRS involving the RNFL of primarily the nasal-superior sector (Figs. 3A–C), which increases over time, peaking two years later (Fig. 3C, time point outlined by red box) and resolving completely after an additional three years. This patient's contralateral eye (Figs. 3D–F) shows PPRS involving the RNFL of the temporal-inferior sector, which appears to develop and resolve completely twice over the span of 5 years of follow-up. This schisis occurred in a sector overlapping an RNFL defect, whose boundary is clear on both infrared reflectance and circumpapillary OCT B-scan images (Figs. 3D–E, red arrowheads). Progressive RNFL thinning is apparent in this sector during the time span over which these events transpire.

Glaucoma Progression Associated With PPRS

Given clear evidence of RNFL thinning shown in the above examples, we sought to determine whether there was an association between PPRS and glaucoma progression overall.

Investigative Ophthalmology & Visual Science

Table. Demographics and Clinical Characteristics of Patients With PPRS and Controls

	PPRS (10 Patients/12 Eyes)		Control (30 Patients/30 Eyes)		
	Average ± SD	Range	Average ± SD	Range	Comparison *P* Value
Age, y	67.3 ± 10.1	47.9 to 80.5	72.6 ± 7.8	58.4 to 88.9	0.15*
Sex, male/female	3/7		5/25		0.57†
BCVA, logMAR	0.07 ± 0.09	0.0 to 0.3	0.09 ± 0.13	0.0 to 0.6	0.91*
CCT, μm	534 ± 41	471 to 585	554 ± 30	478 to 609	0.26*
IOP, mm Hg	17.0 ± 3.3	12 to 21	16.7 ± 4.1	7 to 24	0.83*
IOP at goal (% of eyes)	67%		80%		0.30†
Cup-to-disc ratio	0.81 ± 0.18	0.3 to 0.9	0.73 ± 0.17	0.3 to 0.9	0.06*
SAP MD pre-PPRS, dB	−4.5 ± 4.9	−13.5 to 1.0	−2.1 ± 3.9	−15.5 to 1.7	0.09*
RNFLT pre-PPRS, μm	71.8 ± 10.4	54.0 to 90.0	84.5 ± 18.9	37.5 to 106.3	0.02*

* Mann-Whitney non-parametric rank sum test.
† Fisher's exact test.

First, we analyzed whether progressive RNFL thinning was localized to the same sector of primary PPRS involvement. For this analysis, we included the 8 eyes (of 7 patients) with definitive onset and resolution of PPRS (excluding the visits between those time points). We included the RNFL value for the instrument-defined sector that was primarily involved as well as the RNFL value for the mirrored sector (across the horizontal midline) and calculated the rate of RNFL change over time for each sector.

Although there was significant RNFL thinning in both sectors (that with PPRS and the mirrored opposite sector), there was no significant difference between their rates of progression ($P = 0.39$, paired *t*-test): the average rate of RNFL progression for PPRS sectors was –6.4 μm/year (range, –15 to 5 μm/year; $P = 0.018$), while the average rate of RNFL progression for the mirrored sectors was –4.4 μm/year (range, –12 to 1 μm/year; $P = 0.017$).

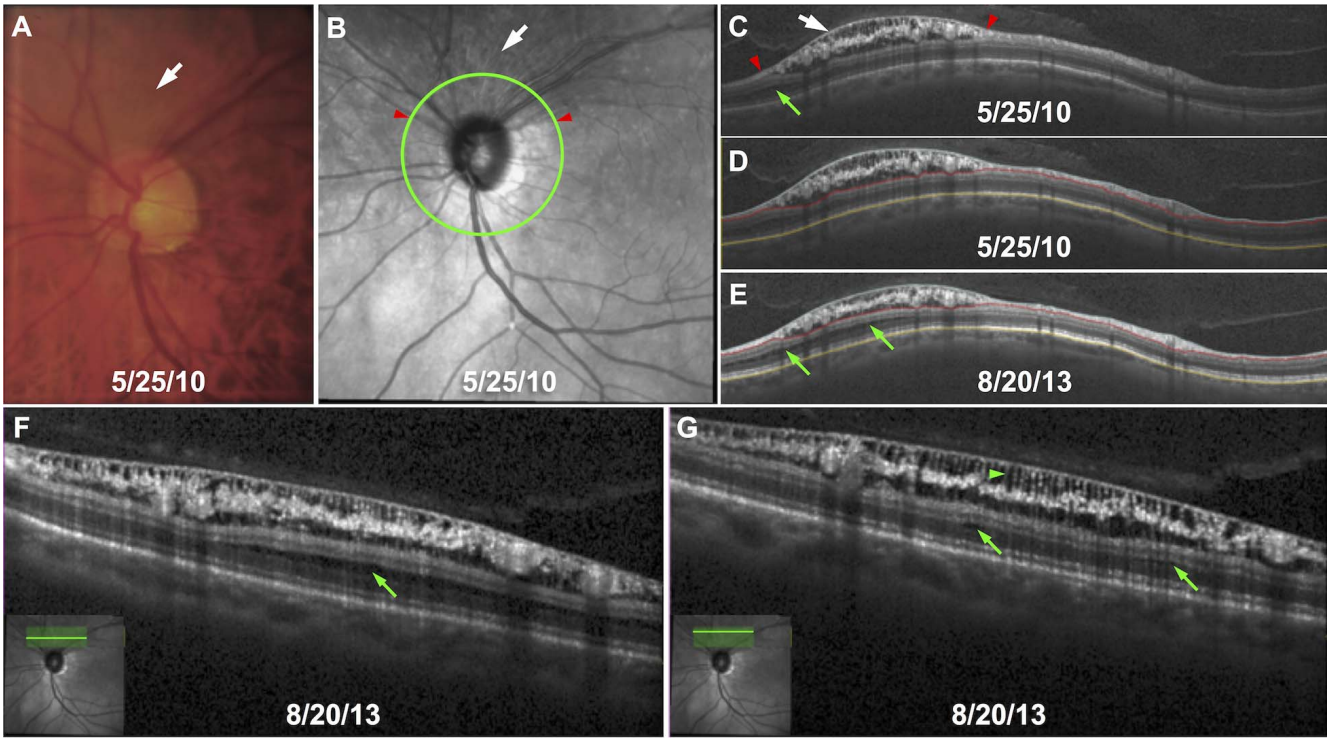

Figure 1. Example of a relatively large peripapillary retinoschisis (PPRS). Peripapillary retinoschisis is typically difficult to discern on optic disc color photographs (**A**, *white arrow*) but is more clearly visible on SLO infrared reflectance images (**B**); in this example case, the area of retinoschisis involves the entire superior pole of the optic disc, having a radial extent of just over 120°, from the 10 o'clock to the 2 o'clock positions, as can be appreciated in the circumpapillary OCT B-scan (**C**, *white arrow*); the red arrowheads demarcate extent of schisis within the inner retina (RNFL and GGL in both [**1B**] and [**1C**]), however, there is also evidence of outer retinal involvement in this eye along the posterior boundary of the OPL (**C**, *green arrow*). The position of the B-scan shown in (**C**) is indicated by the bright green circle in (**B**). The OCT feature segmentations used for RNFL thickness measurements are shown for the same time point in (**D**). Approximately 3 years later (**E**), the depth of the schisis within the inner retina had decreased while the lateral extent of the outer retinal break had become wider. OCT scans consisting of a horizontal raster pattern ([**F**] and [**G**], 49 B-scans spaced approximately 30 μm apart covering a total of 5° height with 768 A-lines per B-scan spanning 15° width) show that the extent of the schisis overall and involvement of each layer vary with distance from the optic disc margin (compare [**F**] to [**G**], ~750 and 1250 μm from the superior disc margin, respectively); *green arrows* point to schisis involving the outer retina; *green arrowhead* points to one of many "bridging structures" crossing the inner retinal schisis.

Investigative Ophthalmology & Visual Science

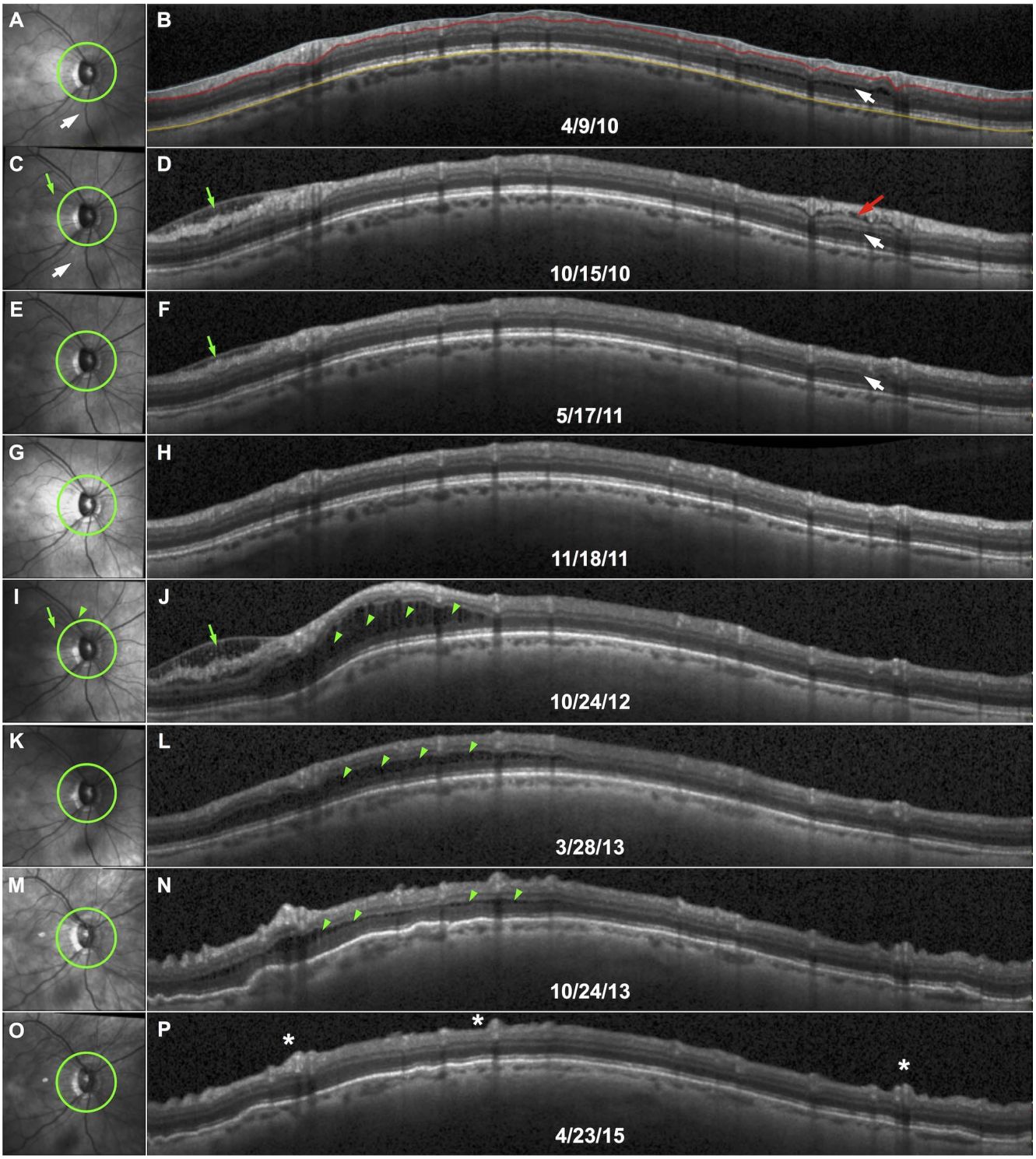

Figure 2. Example of multiple PPRS events in a single eye involving different sectors and retinal layers. *Left column* shows SLO infrared reflectance images and right column shows corresponding OCT circumpapillary B-scans for a series of longitudinal follow-up visits; the position of the OCT B-scan at each time point is indicated by the bright green circle in the SLO image. At study entry, there was evidence of outer retinal schisis (spanning the OPL-ONL boundary) within the inferior quadrant (**A**, **B**, *white arrows*), with little apparent involvement of the inner retina). At the next visit 6 months later, the outer retinal schisis appeared to have narrowed but the inner retina at the same inferior location had clearly become involved (**D**, *red arrow*) and an entirely separate PPRS event had manifest within the RNFL of the temporal-superior sector (**D**, *green arrow*). Both locations gradually resolved over the next year (**F**, **H**), but 6 months later, the same temporal-superior sector RNFL schisis recurred (**J**, *green arrow*) and was contiguous with a severe outer retinal schisis, which spanned nearly the entire superior hemisphere (**J**, *green arrowheads*). This outer retinal schisis took longer to resolve than the RNFL schisis; when both appeared to be completely resolved 2.5 years later, there was clear evidence that progressive RNFL thinning had occurred, including protrusion of the major blood vessels anteriorly toward the vitreous (**P**, *asterisks*).

Investigative Ophthalmology & Visual Science

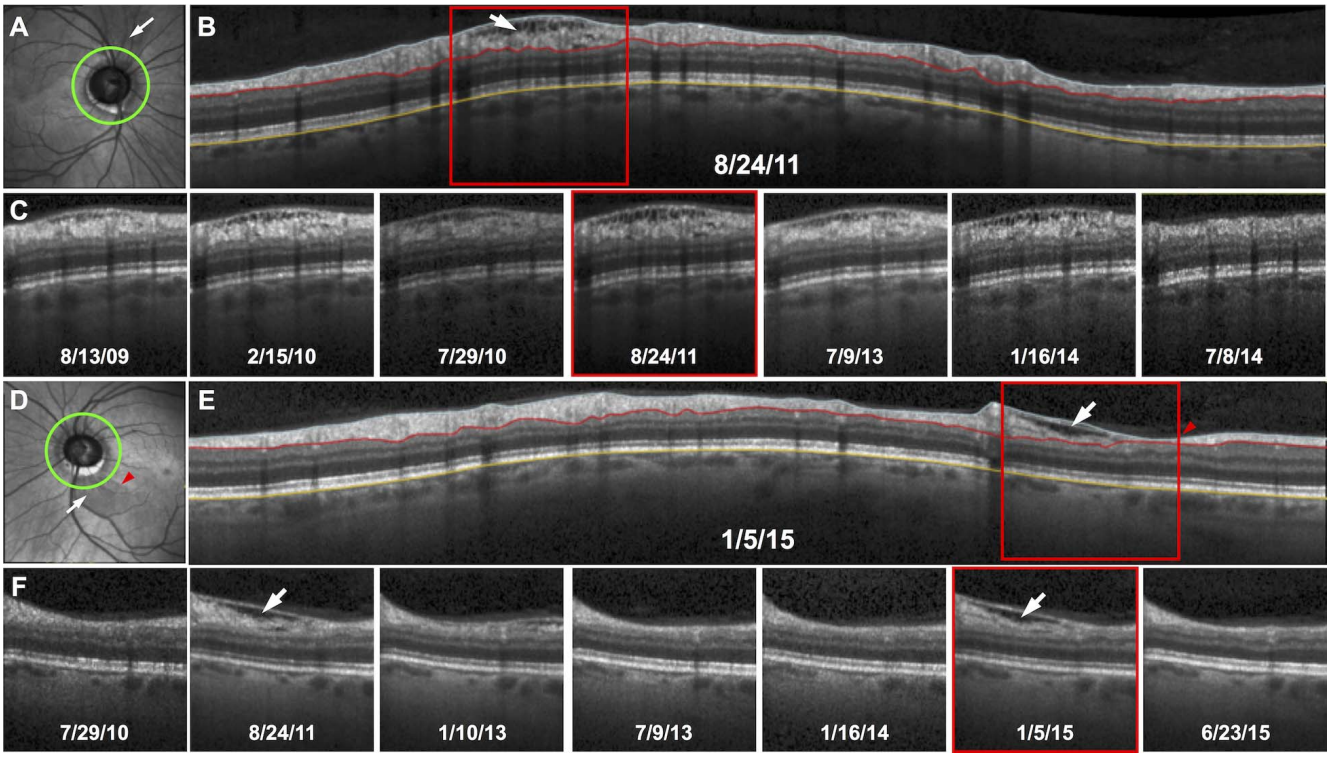

Figure 3. Example of PPRS recurrence and bilateral presentation. A series of longitudinal follow-up circumpapillary OCT B-scans in this patient's right eye (**A**–**C**) shows evidence of PPRS at the first study visit (8/13/2009, leftmost panel in **C**) involving the RNFL primarily within the nasal-superior sector (*white arrows* in **A**, **B**), which increases over time, peaking two years later (**C**, time point outlined by *red box*, 8/24/2011) and resolving completely after an additional three years (**C**, *rightmost panel*, 7/8/2014). This patient's contralateral eye shows PPRS involving the RNFL of the temporal-inferior sector (**D**–**F**, *white arrows*), which appears to develop and resolve completely twice over the span of 5 years of follow-up. This schisis occurred in a sector overlapping an RNFL defect, whose boundary is clear on both infrared reflectance and circumpapillary OCT B-scan images (**D**, **E**, *red arrowheads*). Progressive RNFL thinning is apparent in this sector during the time span over which these events transpire.

Given this evidence that significant RNFL thinning was occurring in both PPRS and mirrored sectors, we compared the rate of change of global average RNFL thickness values in the same PPRS group ($n = 8$ events of 7 eyes) to the rates calculated for the group of 30 control eyes (median of 9 visits; range, 6–11). Global average RNFL thickness progressed more rapidly in PPRS eyes (average rate, −1.9 µm/year; range, −4.4 to −1.1 µm/year) than it did in control eyes (average rate, −1.1 µm/year; range, −4.3 to 0.6 µm/year; comparison $P = 0.043$, GEE). Expressed as a percentage of starting values, the rate of RNFL thinning was also faster in PPRS eyes (average rate, −2.8 %/year; range, −7.4% to 0.0%/year) as compared with control eyes (average rate, −1.3%/year; range, −4.4% to 0.6%/year; comparison $P = 0.021$, GEE).

We performed a similar analysis using values for visual field MD, but including all visual fields collected during the observation period (which should not be biased by the presence of PPRS) to obtain a more accurate estimate of the rate of change. The rate of MD change in PPRS eyes (average, −0.49 dB/year; range, −2.0 to 0.9 dB/year) was significantly faster (more rapid deterioration) than that in control eyes (average, −0.06 dB/year; range, −0.8 to 0.3 dB/year; comparison $P = 0.030$). Accounting for the starting values of MD, the rate of overall visual field deterioration was 6 times faster in PPRS eyes than in control eyes (comparison $P = 0.024$). Analysis of localized visual field change revealed that rates of deterioration within clusters of visual field test locations corresponding to the RNFL bundles of the PPRS sector were not significantly different from the mirrored clusters of the opposite hemifield, consistent with the findings for the sectoral RNFL thickness changes.

Peripapillary Retinoschisis and Association With OCT Signs of Vitreous Adhesion

The presence and absence of posterior vitreous adhesions to the surface of the optic disc or peripapillary retina was assessed by reviewing the vitreoretinal interface on SD-OCT images. OCT evidence of vitreous adhesion was detected in a minority of PPRS cases (13%, 2/15) and controls (16%, 5/30) and thus was not specifically associated with PPRS ($P = 0.57$, Fisher's exact test). When OCT signs of epiretinal membrane with surface wrinkling were included, 27% (4/15) of PPRS eyes and 20% (6/30) of control eyes had signs of either vitreous adhesion or epiretinal membrane with wrinkling, which was not a statistically significant difference ($P = 0.44$, Fisher's exact test).

OCT Signs of Putative Müller Cell Involvement and Activation

One feature prominent in all OCT scans showing PPRS is the presence of so-called "bridging structures" crossing the schisis axially (see Figs. 1–4). These strut-like features also appear to attenuate the OCT signal in a manner similar to blood vessels, casting "shadows" onto the more posterior retinal layers (e.g., Fig. 4D). Anteriorly, these structures expand slightly laterally as they near the ILM, a morphologic feature reminiscent of Müller cells. Similarly, in the majority of instances where OCT B-scans crossed the RNFL bundles perpendicular to their course, these hyperreflective stalks appeared to cross between axon bundles, consistent with Müller cells role in forming the septa between adjacent bundles. In four eyes of four individuals who

Investigative Ophthalmology & Visual Science

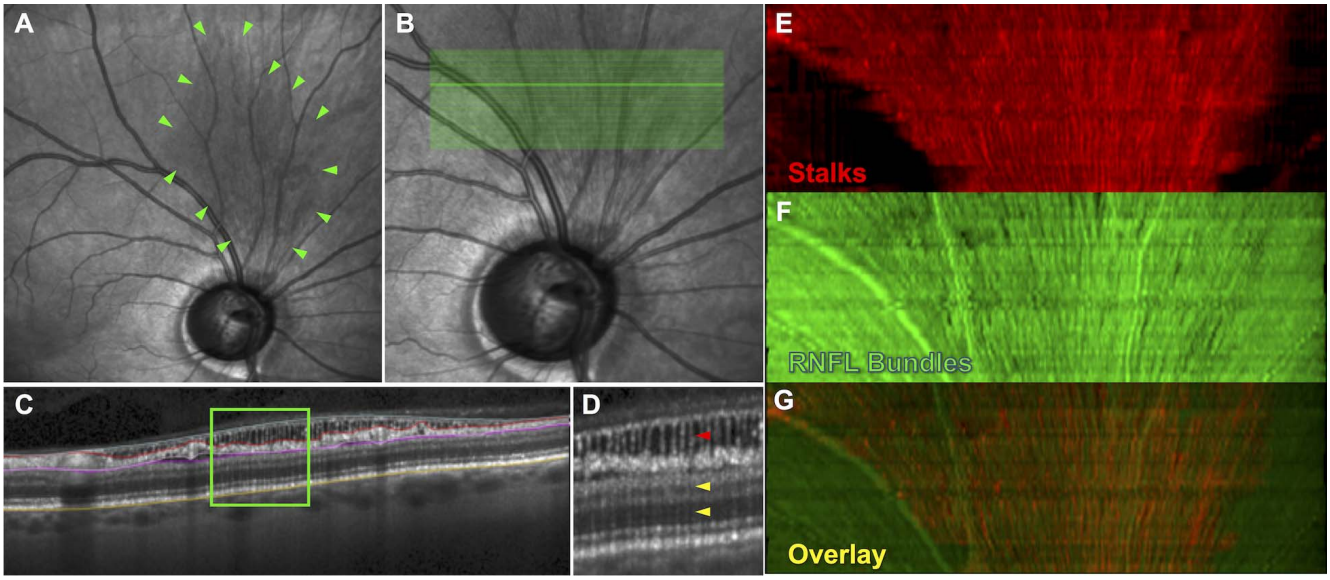

Figure 4. Evidence that the "bridging structures" crossing the schisis in OCT images are Müller cell processes. Alternative OCT B-scan patterns assist to reveal three-dimensional spatial relationships of PPRS features. For example, in this eye (the same eye as shown in Fig. 3A–C), the full extent of PPRS evident in the SLO infrared reflectance image is outlined by green arrowheads (**A**). A horizontal raster pattern of 49 OCT B-scans was obtained over an area spanning 5° vertically by 15° horizontally (**B**, each B-scan was spaced approximately 30 μm apart and consisted of 768 A-lines). We used custom software to delineate OCT image features of each B-scan (**C**), including the ILM (*blue line*), the anterior and posterior boundaries of the RNFL axon bundles (*red* and *pale pink lines*, respectively) and the anterior boundary of the IPL (*magenta line*). From these segmentations, we produced en face slab projection images for the axial depths located between the ILM and anterior RNFL boundary, which contained primarily stalk-like "bridging structures" (**E**) and for axial depths located between the anterior and posterior RNFL boundaries (**F**). The overlay of these two en face projection images (**G**) demonstrates that there is little overlap (unless along the sides of a blood vessel) and that the transverse (lateral) position of the bridging structures is generally located between the RNFL bundles throughout the OCT scan area. This, along with other evidence (see text) suggests that the stalk-like bridging structures crossing the schisis of the inner retina (RNFL and GCL) are the inner processes of Müller cells. Note how the presumed Müller cell processes (magnified inset in **D**, *red arrowhead*) attenuate the OCT signal and cast a "shadow" onto the more posterior retinal layers (**D**, *yellow arrowheads*).

had horizontal raster scans over the PPRS area (i.e., 49 horizontal B-scans spaced approximately 30 μm apart, see for example, Fig. 4), we counted the number of bridging structures crossing the schisis and calculated their average lateral spacing. In these four eyes, respectively, the spacing of bridging structures was 55.6 ± 3.6, 46.7 ± 3.2, 40.8 ± 3.1, and 55.8 ± 5.3 μm. We also used custom software to delineate the following boundaries in each B-scan through the schisis area: the ILM, the anterior and posterior aspects of the axon bundles, the anterior aspect of the inner plexiform layer (IPL) and the Bruch's membrane (BM), as shown in Figure 4. Using these segmentations, we produced en face slab projection images,[39,40] each of which demonstrated that these stalk-like structures lie between axon bundles of the RNFL, consistent with them forming the glial septa in the normal state.

Discussion

In this study we found that PPRS was detected in ~6% of patients diagnosed with primary open angle glaucoma or as glaucoma suspects, similar to estimates from previous reports, which found that PPRS occurs in glaucoma up to 12 times more frequently than in healthy eyes.[20–22] Also similar to previous observations, we found that PPRS is difficult to detect by clinical examination (direct and indirect ophthalmoscopy) or by inspection of stereoscopic color fundus photographs of the optic disc and peripapillary retina; it is more readily detected in SLO infrared reflectance images as a darkened area contiguous with the optic disc with prominent, exaggerated striae following the course of RNFL bundles.[20,21,23] Definitive identification of PPRS is achieved by OCT imaging. We found that PPRS occurred bilaterally in 2/10 individuals (20%), which is similar to the proportion of 11% found in several other studies.[18,22,23] Although only a small discrepancy, the higher proportion of bilateral involvement detected in our study could be the result of our longer duration of follow-up. In addition to bilateral occurrence, we also demonstrate here that multiple PPRS events can occur in the same eye, including separate events at a second peripapillary sector, as reported previously by Hwang and colleagues.[18] However, our study demonstrates that PPRS can resolve completely then recur at the same location, which has not been previously shown. We also here extend previous knowledge by finding that PPRS is associated with a more rapid rate of overall progression measured both by circumpapillary RNFL thickness and by SAP visual field MD compared with glaucomatous and glaucoma suspect eyes that do not have PPRS. In fact, eyes with PPRS progressed at a rate that was twice as fast as controls as measured by global average RNFL thickness and 4–6 times faster than controls as measured by visual field MD. Finally, we also demonstrate evidence of Müller cell involvement in the process of glaucomatous PPRS detectable by OCT imaging.

Our observation that glaucoma progression was faster in eyes with PPRS conflicts with one prior study that reported no significant differences between values of quadrant or global average RNFL thickness, or visual field indices after PPRS resolution as compared with values prior to PPRS.[18] However, that conclusion by Hwang et al.[18] was drawn on the basis of a smaller sample (5 eyes) and did not consider rates of change as we did, which could be important given the variable duration PPRS can have in different eyes. Another study has reported only transient worsening of visual field sensitivity during the active phase of PPRS, without evidence of permanent or

continued progression.[20] One interesting possibility is that the association we found between PPRS and faster glaucoma progression reflects pathogenesis of PPRS.

For example, it is possible that glaucomatous ONH deformation, with posterior displacement of the ONH tissues deeper into the scleral canal exerts lateral mechanical forces on the peripapillary inner retina, which may be exacerbated by additional (perhaps opposing) tractional forces exerted by the vitreous. If these forces overwhelm the mechanical tensile strength of the retina, it could ultimately result in schisis formation. This is generally supported by the finding that PPRS is substantially more common in glaucomatous eyes than in age-similar healthy eyes (which presumably have a similar rate of posterior vitreous detachment), as well as by the report that structural defects of the lamina cribrosa are associated with glaucomatous PPRS.[26] Although we observed that some instances of PPRS were concurrent with signs of focal vitreous adhesion visible with OCT, this was not a specific finding for PPRS because there were more instances of PPRS without any such signs, similar to the findings of another study.[23] One caveat is that we noted some cases in which the circumpapillary OCT B-scan did not reveal any sign of vitreous adhesion whereas one or more of the radial B-scans through the ONH did (either distal or proximal to the location of the circumpapillary B-scan). Thus, it is possible that a denser OCT scan pattern would uncover a larger proportion of PPRS cases with evidence of vitreous traction.[25] Nevertheless, it is possible that glaucomatous ONH deformation, which can include posterior displacement of the lamina cribrosa and ONH surface as large as a few hundred micrometers, exerts active lateral traction on the inner retina, which could overcome its tensile strength to create PPRS even in the absence of vitreous traction. Indeed, it is well known that the position of the major blood vessel trunks move with glaucomatous ONH deformation.[41,42] Thus it may be that defects observed along blood vessels represent a similar interplay of mechanical forces.[43]

Consistent with this theory is our finding that eyes with PPRS tend to have a more advanced stage of glaucoma and are undergoing more rapid progression over the time span when PPRS occurs. A study by Lee et al.[21] has also reported that eyes with PPRS have more advanced visual field damage compared to glaucomatous eyes without PPRS. Moreover, several studies, including ours, have reported that PPRS occurs either exclusively or at least predominantly at the same sector as existing RNFL bundle defects.[20,21] In addition to the mechanical forces potentially exerted on the peripapillary retina by glaucomatous ONH deformation, it is also possible that glaucoma alters Müller cell structure or function. Müller cells are known to respond rapidly and specifically to mechanical stretch of the retina with transient increases of intracellular calcium and changes in protein expression.[44] It has also been shown that Müller cells exhibit signs of reactive gliosis in glaucoma such as upregulation of the intermediate filament GFAP (glial fibrillary acidic protein).[30,45] Among other critical functions, Müller cells are known to act like springs, providing essential mechanical strength against dynamic shear and tensile forces that buffet the retina throughout life.[31] Ablating the Müller glia from the developing mouse retina causes it to rip apart at the level of the GCL in maturity.[31] Furthermore, it is the intermediate filaments in particular, within the inner portion and endfeet of Müller cells, which are thought to provide the resistance to mechanical stress.[46] Indeed, for decades it has been postulated that Müller cells have a role in the pathogenesis of retinoschisis.[2,28,29,47]

In light of this background, it is pertinent that we demonstrate here evidence of Müller cell involvement in glaucomatous PPRS. First, in every instance of PPRS, the OCT images showed that the schisis cavity was spanned by hyperreflective strut-like pillars described by other authors as "bridging structures"[14] and visible (if not mentioned) in the OCT images of other previous publications on PPRS.[18,20,21,23] We measured that the spacing of these stalk-like structures was consistently ~50 μm, which matches closely the spacing of Müller cell profiles crossing the RNFL in histologic material[48,49] and highlight that they flair out laterally within a few micrometers of the ILM, consistent with the morphology of Müller cell endfeet.[48] Further, we demonstrate that these hyper-reflective stalks cast "shadows" onto the distal retinal layers in a manner similar to the strong signal attenuation produced by blood vessels. Taken together, this constellation of OCT signs is strongly suggestive Müller cell reactive gliosis, although it is also possible that the change in morphology (stretch) alters the waveguide characteristics normally exhibited by Müller cells.[50] These OCT findings in vivo are similar to the histologic findings reported previously for retinoschisis.[6,28,29] What remains to be determined is whether intrinsic or acquired Müller cell dysfunction is contributory to glaucomatous PPRS or that these OCT signs of 'activated' Müller cells represent their response to mechanical stress. In either case, reactive gliosis (reflected as these OCT signs) and/or dramatic alteration of Müller cell morphology might lead to altered physiologic function and "aggravate neurodegeneration within the cystic tissue."[47] Hence, we plan to systematically survey OCT scans from glaucomatous human eyes to seek for this shadow sign of Müller cell gliosis even in the absence of schisis. In this context, one important caveat to note is that we have observed similar banding patterns of outer retinal reflectance on OCT scans of eyes with so-called "microcystic edema" of the inner nuclear layer (INL), for example, in nonhuman primate eyes with idiopathic bilateral optic atrophy (Fig. 5).[35,36] However, the origin of this phenomenon is somewhat different in that the brighter bands appear to result from decreased attenuation and scatter through the voids ("microcysts") relative to the adjacent, intact retina (Fig. 5). Yet it remains likely that the development of such "microcysts" involves a similar interaction between mechanical forces and Müller cell biophysics (which tend to maintain the intrinsic thickness of the previously healthy retina);[51,52] it is interesting that INL microcysts tend to form where the inner retina is thickest in the healthy state, and generally only when those areas degenerate (lose tissue) rapidly.

There are limitations in this study that may impact our conclusions. First, the ongoing longitudinal P3 study includes radial ONH and circumpapillary OCT scans, which may limit complete characterization of the extent of PPRS and detection of vitreoretinal or vitreopapillary traction. In several cases of PPRS detected by inspection of those standard OCT scan types, we subsequently included denser raster scan patterns which revealed more detail about the extent of schisis and the retinal layers involved. Similarly, there was evidence of vitreoretinal adhesion present in some OCT B-scans crossing the area of PPRS but not others. Thus, it is possible that the proportion of glaucomatous and suspect eyes with PPRS is even higher than we and others have estimated and/or that vitreous traction plays an even more important pathogenic role. Second, although the relatively long time span of regular follow-up visits enabled us to provide estimates of PPRS duration and to detect multiple PPRS events within individual patients (bilateral cases as well as recurrence within a sector and at other sectors of the same eye), the visits were still separated by 6 months. Thus, it is possible that more frequent testing would refine estimates of duration and reveal a higher proportion of glaucomatous eyes with PPRS. Furthermore, the relatively small number of eyes with PPRS that we studied (12 eyes of 10 patients) limits the precision with which we can estimate the relative likelihood and rate of glaucoma progression

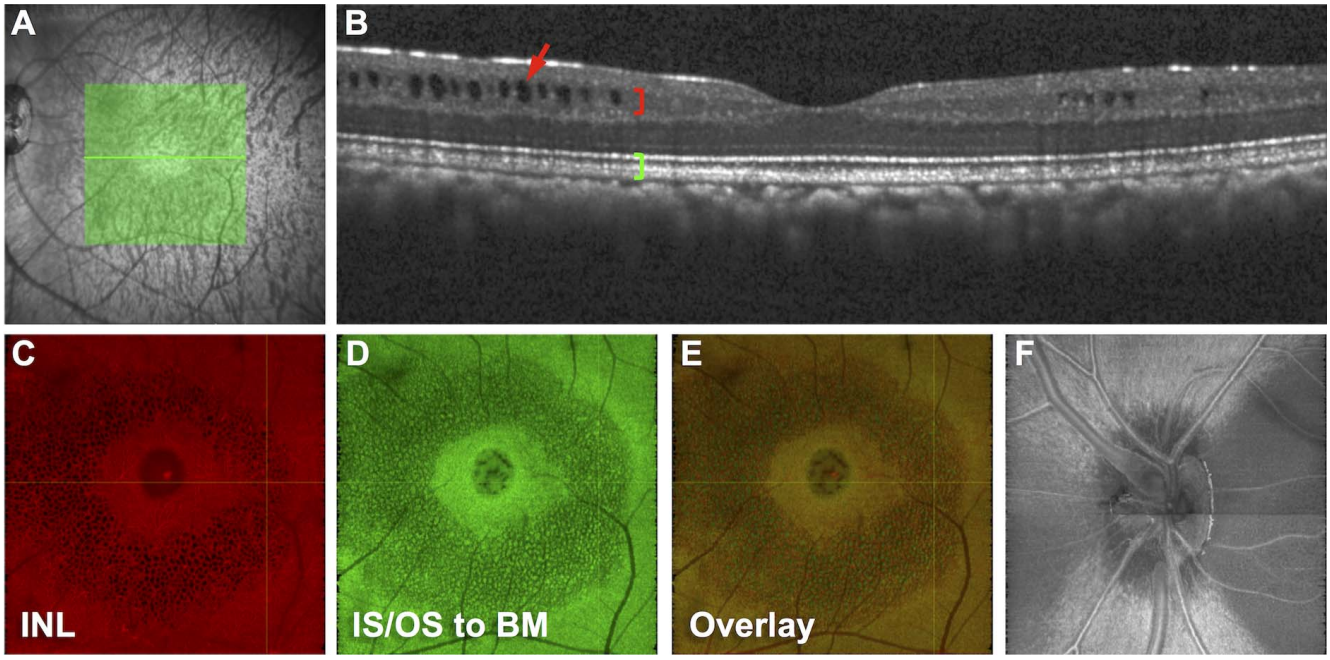

FIGURE 5. "Microcystic" degeneration of the INL may also cause OCT reflectivity banding of the outer retina. An example of microcystic degeneration of the INL, in this case from the left eye of a non-human primate with bilateral idiopathic optic atrophy, causing reflectivity banding of the outer retina. OCT horizontal raster scan pattern consisting of 290 B-scans over a $10° \times 10°$ area of the macula (*green lines*) shown overlaid onto the SLO infrared reflectance image (**A**). OCT B-scan through the fovea (**B**) from the location corresponding to the *bright green line* in A; note numerous "microcysts" present throughout the INL (*red arrow*) as well as the reflectivity banding pattern present throughout the portions of the outer retinal layers corresponding to microcystic degeneration of the INL. (**C**) En face slab projection image of the INL (corresponding to the red bracket in **B**), showing microcysts distributed throughout the areas of the macula where the RGC layer is thickest. (**D**) En face slab projection image of the outer retina (from the inner segment/outer segment junction, IS/OS, to BM; note how the center of each area posterior to an INL microcyst exhibits more intense reflectivity (is brighter) than the surrounding retina. (**E**) Overlay of C and D to demonstrate spatial correspondence of microcysts with brighter areas of outer retinal reflectivity (and possibly darker areas representing attenuation by retina immediately surrounding each microcyst). (**F**) En face slab projection image for a separate 290-B-scan pattern centered over the optic disc (produced as the sum of 30 voxels, ~115 μm in depth, beginning 6 voxels, ~23 μm, below the ILM) shows the characteristic "butterfly" pattern of axon loss affecting the temporal and nasal quadrants; microcysts of the macular INL are visible on the temporal side.

associated with PPRS. Thus, additional studies are needed to further evaluate the association between PPRS and glaucoma progression.

In summary, we demonstrate for the first time that glaucomatous PPRS is associated with a faster rate of glaucoma progression measured either by global average circumpapillary RNFL thickness or by visual field MD as compared with a control group of glaucomatous and suspect eyes without PPRS. We further demonstrate that OCT imaging reveals signs of Müller cell involvement in the pathogenesis of glaucomatous PPRS.

Acknowledgments

The authors thank Cindy Albert for expert technical assistance during data collection and Juan Reynaud for software development.

Supported by Grant R01-EY019674 (SD) and the Legacy Good Samaritan Foundation.

Disclosure: **B. Fortune**, None; **K.N. Ma**, None; **S.K. Gardiner**, None; **S. Demirel**, None; **S.L. Mansberger**, None

References

1. Sauer CG, Gehrig A, Warneke-Wittstock R, et al. Positional cloning of the gene associated with X-linked juvenile retinoschisis. *Nat Genet*. 1997;17:164–170.
2. Mooy CM, Van Den Born LI, Baarsma S, et al. Hereditary X-linked juvenile retinoschisis: a review of the role of Müller cells. *Arch Ophthalmol*. 2002;120:979–984.
3. Byrne LC, Ozturk BE, Lee T, et al. Retinoschisin gene therapy in photoreceptors, Müller glia or all retinal cells in the Rs1h-/- mouse. *Gene Ther*. 2014;21:585–592.
4. Molday RS, Kellner U, Weber BH. X-linked juvenile retinoschisis: clinical diagnosis, genetic analysis, and molecular mechanisms. *Prog Retin Eye Res*. 2012;31:195–212.
5. Byer NE. Clinical study of senile retinoschisis. *Arch Ophthalmol*. 1968;79:36–44.
6. Straatsma BR, Foss RY. Typical and reticular degenerative retinoschisis. *Am J Ophthalmol*. 1973;75:551–575.
7. Georgalas I, Ladas I, Georgopoulos G, Petrou P. Optic disc pit: a review. *Graefes Arch Clin Exp Ophthalmol*. 2011;249:1113–1122.
8. Hotta K, Hirakata A, Hida T. Retinoschisis associated with disc coloboma. *Br J Ophthalmol*. 1999;83:124.
9. Benhamou N, Massin P, Haouchine B, Erginay A, Gaudric A. Macular retinoschisis in highly myopic eyes. *Am J Ophthalmol*. 2002;133:794–800.
10. Rutledge BK, Puliafito CA, Duker JS, Hee MR, Cox MS. Optical coherence tomography of macular lesions associated with optic nerve head pits. *Ophthalmology*. 1996;103:1047–1053.
11. Spaide RF, Costa DL, Huang SJ. Macular schisis in a patient without an optic disk pit optical coherence tomographic findings. *Retina*. 2003;23:238–240.
12. Hollander DA, Barricks ME, Duncan JL, Irvine AR. Macular schisis detachment associated with angle-closure glaucoma. *Arch Ophthalmol*. 2005;123:270–272.

13. Kahook MY, Noecker RJ, Ishikawa H, et al. Peripapillary schisis in glaucoma patients with narrow angles and increased intraocular pressure. *Am J Ophthalmol*. 2007;143:697–699.
14. Zumbro DS, Jampol LM, Folk JC, Olivier MM, Anderson-Nelson S. Macular schisis and detachment associated with presumed acquired enlarged optic nerve head cups. *Am J Ophthalmol*. 2007;144:70–74.
15. Hubschman JP, Reddy S, Kaines A, Law S. Nasal retinoschisis associated with glaucoma. *Ophthalmic Surg Lasers Imaging*. 2010;1–4.
16. Zhao M, Li X. Macular retinoschisis associated with normal tension glaucoma. *Graefes Arch Clin Exp Ophthalmol*. 2011; 249:1255–1258.
17. Farjad H, Besada E, Frauens BJ. Peripapillary schisis with serous detachment in advanced glaucoma. *Optom Vis Sci*. 2010;87:E205–E217.
18. Hwang YH, Kim YY, Kim HK, Sohn YH. Effect of peripapillary retinoschisis on retinal nerve fibre layer thickness measurement in glaucomatous eyes. *Br J Ophthalmol*. 2014;98:669–674.
19. Inoue M, Itoh Y, Rii T, et al. Spontaneous resolution of peripapillary retinoschisis associated with glaucomatous optic neuropathy. *Acta Ophthalmol*. 2015;93:e317–318.
20. van der Schoot J, Vermeer KA, Lemij HG. Transient peripapillary retinoschisis in glaucomatous eyes. *J Ophthalmol*. 2017;2017:1536030.
21. Lee EJ, Kim TW, Kim M, Choi YJ. Peripapillary retinoschisis in glaucomatous eyes. *PLoS One*. 2014;9:e90129.
22. Bayraktar S, Cebeci Z, Kabaalioglu M, Ciloglu S, Kir N, Izgi B. Peripapillary retinoschisis in glaucoma patients. *J Ophthalmol*. 2016;2016:1612720.
23. Dhingra N, Manoharan R, Gill S, Nagar M. Peripapillary schisis in open-angle glaucoma. *Eye (Lond)*. 2017;31:499–502.
24. Inoue M, Itoh Y, Rii T, et al. Macular retinoschisis associated with glaucomatous optic neuropathy in eyes with normal intraocular pressure. *Graefes Arch Clin Exp Ophthalmol*. 2015;253:1447–1456.
25. Grewal DS, Merlau DJ, Giri P, et al. Peripapillary retinal splitting visualized on OCT in glaucoma and glaucoma suspect patients. *PLoS One*. 2017;12:e0182816.
26. Lee JH, Park HY, Baek J, Lee WK. Alterations of the lamina cribrosa are associated with peripapillary retinoschisis in glaucoma and pachychoroid spectrum disease. *Ophthalmology*. 2016;123:2066–2076.
27. Patel S, Ling J, Kim SJ, Schey KL, Rose K, Kuchtey RW. Proteomic analysis of macular fluid associated with advanced glaucomatous excavation. *JAMA Ophthalmol*. 2016;134:108–110.
28. Yanoff M, Kertesz Rahn E, Zimmerman LE. Histopathology of juvenile retinoschisis. *Arch Ophthalmol*. 1968;79:49–53.
29. Kirsch LS, Brownstein S, de Wolff-Rouendaal D. A histopathological, ultrastructural and immunohistochemical study of congenital hereditary retinoschisis. *Can J Ophthalmol*. 1996; 31:301–310.
30. Wang L, Cioffi GA, Cull G, Dong J, Fortune B. Immunohistologic evidence for retinal glial cell changes in human glaucoma. *Invest Ophthalmol Vis Sci*. 2002;43:1088–1094.
31. MacDonald RB, Randlett O, Oswald J, Yoshimatsu T, Franze K, Harris WA. Müller glia provide essential tensile strength to the developing retina. *J Cell Biol*. 2015;210:1075–1083.
32. Gardiner SK, Johnson CA, Demirel S. Factors predicting the rate of functional progression in early and suspected glaucoma. *Invest Ophthalmol Vis Sci*. 2012;53:3598–3604.
33. Gardiner SK, Boey PY, Yang H, Fortune B, Burgoyne CF, Demirel S. Structural Measurements for monitoring change in glaucoma: comparing retinal nerve fiber layer thickness with minimum rim width and area. *Invest Ophthalmol Vis Sci*. 2015;56:6886–6891.
34. Mansberger SL, Menda SA, Fortune BA, Gardiner SK, Demirel S. Automated segmentation errors when using optical coherence tomography to measure retinal nerve fiber layer thickness in glaucoma. *Am J Ophthalmol*. 2017;174:1–8.
35. Fortune B, Wang L, Bui BV, Burgoyne CF, Cioffi GA. Idiopathic bilateral optic atrophy in the rhesus macaque. *Invest Ophthalmol Vis Sci*. 2005;46:3943–3956.
36. Piper C, Fortune B, Cull G, Cioffi GA, Wang L. Basal blood flow and autoregulation changes in the optic nerve of rhesus monkeys with idiopathic bilateral optic atrophy. *Invest Ophthalmol Vis Sci*. 2013;54:714–721.
37. Fortune B, Cull GA, Burgoyne CF. Relative course of retinal nerve fiber layer birefringence and thickness and retinal function changes after optic nerve transection. *Invest Ophthalmol Vis Sci*. 2008;49:4444–4452.
38. Tan O, Liu L, Zhang X, Morrison JC, Huang D. Glaucoma increases retinal surface contour variability as measured by optical coherence tomography. *Invest Ophthalmol Vis Sci*. 2016;57:OCT438–443.
39. Fortune B. In vivo imaging methods to assess glaucomatous optic neuropathy. *Exp Eye Res*. 2015;141:139–153.
40. Hood DC, Fortune B, Mavrommatis MA, et al. Details of glaucomatous damage are better seen on OCT en face images than on OCT retinal nerve fiber layer thickness maps. *Invest Ophthalmol Vis Sci*. 2015;56:6208–6216.
41. Radcliffe NM, Smith SD, Syed ZA, et al. Retinal blood vessel positional shifts and glaucoma progression. *Ophthalmology*. 2014;121:842–848.
42. Kuroda A, Enomoto N, Ishida K, et al. Movement of retinal vessels toward the optic nerve head after increasing intraocular pressure in monkey eyes with experimental glaucoma. *Exp Eye Res*. 2017;162:110–115.
43. Hood DC, De Cuir N, Mavrommatis MA, et al. Defects along blood vessels in glaucoma suspects and patients. *Invest Ophthalmol Vis Sci*. 2016;57:1680–1686.
44. Lindqvist N, Liu Q, Zajadacz J, Franze K, Reichenbach A. Retinal glial (Müller) cells: sensing and responding to tissue stretch. *Invest Ophthalmol Vis Sci*. 2010;51:1683–1690.
45. Seitz R, Ohlmann A, Tamm ER. The role of Müller glia and microglia in glaucoma. *Cell Tissue Res*. 2013;353:339–345.
46. Lundkvist A, Reichenbach A, Betsholtz C, Carmeliet P, Wolburg H, Pekny M. Under stress, the absence of intermediate filaments from Müller cells in the retina has structural and functional consequences. *J Cell Sci*. 2004;117:3481–3488.
47. Bringmann A, Pannicke T, Grosche J, et al. Müller cells in the healthy and diseased retina. *Prog Retin Eye Res*. 2006;25:397–424.
48. Hogan MJ, Alvarado JA, Weddell JE. *Histology of the Human Eye*. Philadelphia, PA: Saunders; 1971.
49. Frenkel S, Goshen G, Leach L, Pe'er J, Mimouni M, Blumenthal EZ. Peripapillary distribution of Müller cells within the retinal nerve fiber layer in human eyes. *Exp Eye Res*. 2018;166:91–95.
50. Franze K, Grosche J, Skatchkov SN, et al. Müller cells are living optical fibers in the vertebrate retina. *Proc Natl Acad Sci U S A*. 2007;104:8287–8292.
51. Hasegawa T, Akagi T, Yoshikawa M, et al. Microcystic inner nuclear layer changes and retinal nerve fiber layer defects in eyes with glaucoma. *PLoS One*. 2015;10:e0130175.
52. Lujan BJ, Horton JC. Microcysts in the inner nuclear layer from optic atrophy are caused by retrograde trans-synaptic degeneration combined with vitreous traction on the retinal surface. *Brain*. 2013;136:e260.

Investigative Ophthalmology & Visual Science